Submitted to AJ on March 7th, 2006; Revised May 14, 2006

Comet 162P/Siding Spring: A Surprisingly Large Nucleus

Y. R. Fernández[1,2]

Dept. of Physics, Univ. of Central Florida, 4000 Central Florida Blvd., Orlando, FL 32816-2385

yan@physics.ucf.edu

H. Campins[2]

Dept. of Physics, Univ. of Central Florida, 4000 Central Florida Blvd., Orlando, FL 32816-2385; Lunar and Planetary Laboratory, Univ. of Arizona, 1629 E. University Blvd., Tucson, AZ 85721

M. Kassis[2]

W. M. Keck Observatory, 65-1120 Mamalahoa Hwy, Kamuela, HI 96743

C. W. Hergenrother

Lunar and Planetary Laboratory, Univ. of Arizona, 1629 E. University Blvd., Tucson, AZ 85721

R. P. Binzel

Massachusetts Institute of Technology, 77 Massachusetts Ave., Cambridge, MA 02139

J. Licandro

Isaac Newton Group, P.O. Box 321, 38700, Santa Cruz de La Palma, Tenerife, Spain; Instituto de Astrofísica de Canarias, c/Vía Láctea s/n, 38205, La Laguna, Tenerife, Spain

J. L. Hora

Harvard-Smithsonian Center for Astrophysics, 60 Garden St., MS 65, Cambridge, MA 02138-1516

J. D. Adams

Dept. of Astronomy, Cornell University, Ithaca, NY 14853

ABSTRACT

We present an analysis of thermal emission from comet 162P/Siding Spring (P/2004 TU_{12}) measured during its discovery apparition in December 2004. The comet showed no dust coma at this time, so we have sampled emission from the comet's nucleus. Observations using the "Mid-Infrared Spectrometer and Imager" ("MIRSI") were performed at NASA's Infrared Telescope Facility, where the peak of the comet's spectral energy distribution was observed between 8 and 25 μm. In combination with the three near-infrared spectra presented by Campins *et al.* (2006, *AJ*, this issue) that show the Wien-law tail of the thermal emission, the data provide powerful constraints on surface properties of the nucleus. We find that the nucleus's effective radius is 6.0 ± 0.8 km. This is one of the largest radii known among Jupiter-family comets, which is unusual considering the comet was discovered only recently. Its geometric albedo is 0.059 ± 0.023 in H-band, 0.037 ± 0.014 in R-band, and 0.034 ± 0.013 in V-band. We also find that the nucleus of 162P has little infrared beaming, and this implies the nucleus has low thermal inertia. Including all near-IR spectra yields a beaming parameter η of 1.01 ± 0.20. This result is in agreement with others showing that cometary nuclei have low thermal inertia and little infrared beaming. If confirmed for many nuclei, the interpretation of radiometry may not be as problematic as feared.

Subject headings: comets: individual (162P) — infrared: solar system

1. Introduction

A narrative of the discovery and morphological evolution of comet 162P is given by Campins et al. (2006) in a companion paper (hereafter Paper I). The thin tail and lack of coma strongly suggested that observations of this comet would reveal flux from the nucleus. Since opportunities to directly study a cometary nucleus are infrequent, our group set up a multiwavelength observing campaign to take advantage of the comet's unusual behavior and probe the reflectance and thermal properties of the nucleus. Paper I addressed the near-infrared spectroscopic properties; in this paper we describe the thermal emission and

[1]Former address: Institute for Astronomy, University of Hawaii, 2680 Woodlawn Dr., Honolulu, HI 96822.

[2]Visiting Astronomer at the Infrared Telescope Facility, which is operated by the University of Hawaii under contract to the National Aeronautics and Space Administration.

the albedo, which include observations from the Wien-law tail through the black-body peak in wavelength.

2. Observations and Reduction

The mid-infrared observations were obtained at NASA's Infrared Telescope Facility between UT 0600 and 0700 on December 27, 2004, using the "Mid-Infrared Spectrometer and Imager" – "MIRSI" – instrument (Deutsch et al. 2002). Conditions were clear and photometric, but only moderately dry. The comet was 1.348 AU from the Sun, 0.777 AU from Earth, and at a phase angle of 46.1 degrees. Chopping and nodding were employed in such a way as to leave four images of the comet on the detector, effectively boosting our signal-to-noise by a factor of 2. The comet appeared as a point-source and there is no chance that we were chopping onto coma. The comet was located just 12.7° away from the standard star β And in the sky, which was used as an absolute flux calibrator. During its observations, the airmass of β And was 1.05 to 1.14. During the observations of 162P, the airmass was 1.14 to 1.19 and then later 1.31 to 1.36. Both comet and star were observed at four wavelengths, 8.7, 9.8, 11.7, and 24.5 μm. The filters through which we observed the comet and the star at significantly different airmasses ($\sim$0.2) were 8.7 and 11.7 μm. However, this airmass difference appeared to be not important: the 11.7 μm flux density was measured at the two airmass values and not found to differ significantly. Since 8.7 μm is a relatively clean part of the N-band, we applied no airmass correction. Given the uncertainty of the photometry (below), this assumption is valid.

MIRSI's filters at the four wavelengths are about 10% wide. We assumed that β And had flux densities of 351.0, 279.3, 198.2, and 46.0 Jy at the four wavelengths, based on the results of Cohen et al. (1996) using the functions of Engelke (1992). Aperture photometry of the comet yielded instrumental magnitudes, which we corrected for aperture size. We calculated absolute flux densities for the comet of 2.0 ± 0.4 Jy, 2.3 ± 0.4 Jy, 2.6 ± 0.4 Jy, and 2.5 ± 0.6 Jy at the four wavelengths.

In addition to our mid-IR data we make use of the near-IR spectra described in Paper I. The spectra were obtained at December 3.25, 10.25, and 11.88 of 2004 (UT). Also we use visible-wavelength photometry published by Hergenrother (2006). Those observations were obtained on November 19.16 and December 9.19 of 2004, and April 6.15 of 2005 (all UT).

3. Analysis

The near-infrared spectra were not flux-calibrated on an absolute scale. Hence we used a two-pronged approach in analyzing the data. Step 1 was to attack just the *absolute* photometry in the mid-IR and visible wavelengths. Step 2 was to analyze just the *relative* fluxes in the near-IR spectra. We describe these below.

3.1. Absolute Photometry

The basic radiometric method to obtain an effective radius, R, and geometric albedo, p, is to solve two equations with these two unknowns, first done about 35 years ago (Allen 1970; Matson 1971; Morrison 1973) and described in detail by Lebofsky & Spencer (1989):

$$F_{vis}(\lambda_{vis}) = \frac{F_\odot(\lambda_{vis})}{(r/1\mathrm{AU})^2}\ R^2 p \frac{\Phi_{vis}(\alpha)}{\Delta^2}, \tag{1a}$$

$$F_{mir}(\lambda_{mir}) = \epsilon \int B_\nu(T(pq,\eta,\epsilon,\theta,\phi),\lambda_{mir}) d\phi d\cos\theta\ R^2\ \frac{\Phi_{mir}(\alpha)}{\pi\Delta^2}, \tag{1b}$$

where F is the measured flux density of the object at wavelength λ in the visible ("vis") or mid-infrared ("mir"); $F_\odot$ is the flux density of the Sun at Earth as a function of wavelength; r and Δ are the object's heliocentric and geocentric distances, respectively; Φ is the phase darkening in each regime as a function of phase angle α; B_ν is the Planck function; ϵ is the infrared emissivity; η is a factor to account for infrared beaming; and T is the temperature. The temperature itself is a function of p, ϵ, η, surface planetographic coordinates θ and ϕ, and the (dimensionless) phase integral q which links the geometric and Bond albedos. For lack of detailed shape information, the modeled body is assumed to be spherical, so all radii given here are "effective" radii.

The surface map of temperature is calculated using a model of the thermal behavior. A simple thermal model covering an extreme of thermal behavior is often employed (Lebofsky & Spencer 1989). This model, the "standard thermal model" (STM), is widely used so results are easy to compare. It applies if the rotation is so slow or the thermal inertia so low that every point on the surface is in instantaneous equilibrium with the impinging solar radiation. In this case the temperature is a maximum at the subsolar point and decreases as $\sqrt[4]{\cos\vartheta}$, where ϑ is the local solar zenith angle. We will show below that the modeling results are consistent with this assumption.

The other parameters to the model are ϵ, Φ_{mir}, Φ_{vis}, q, and η. We have sidestepped the need to explicitly assume values of Φ_{vis} and q by using the nucleus's absolute magnitude H (see below). Emissivity for rocks is close to unity (Morrison 1973) and we assume $\epsilon = 0.9$

here. The choices of Φ_{mir} and η are often the most important determinants in deriving an accurate R and p. We have used the NEA Thermal Model (NEATM) devised by Harris (1998) to determine what to use for these quantities. This model's characterization of Φ_{mir} and η is the primary distinguishing difference from the pure STM. For Φ_{mir}, Harris (1998) argued that a more sophisticated phase law is needed rather than the usual linear phase coefficient. His approach is to calculate a phase effect based simply on the surface-integral of the thermal flux over the Earth-facing hemisphere.

As for η, the standard value of 0.756 (Lebofsky et al. 1986) was originally derived for Ceres. However recent work (Harris 1998; Harris, Davies, & Green 1998; Harris & Davies 1999; Delbó et al. 2003) indicates that small bodies can have a variety of values for η. Thus we have made the beaming parameter a variable to be fit, and our modeling routines return values for three physical parameters, R, p, and η.

We have four mid-IR photometry points, but we need at least one reflected-sunlight measurement. Ideally this measurement would have taken place simultaneously, but unfortunately no such data were taken. Instead we make use of R-band photometry published by Hergenrother (2006). With their measurements taken over a range of phase angles, we derive an R-band absolute magnitude H_R of 13.74 ± 0.25 and a phase slope parameter G of 0.15 ± 0.10 (Bowell et al. 1989). With this photometric constraint, we now effectively have five total measurements to fit three parameters, which leaves us with two degrees of freedom.

The results of the modeling are given in Figs. 1 and 2. Figure 1 displays contour plots for three representative values of η: 0.75, 1.0, and 1.25. The contours trace out the 1, 1.5, 2, 2.5, and 3-σ levels for χ^2_ν. We found the full 1-σ ranges of the three parameters to be as follows: 3.4 km $< R <$ 6.8 km, $0.022 < p_R < 0.102$, and $0.30 < \eta < 1.29$. These are fairly wide and poorly constrained intervals, but we note that the values are highly correlated. This is demonstrated in Fig. 2, where the best-fitting values of R and p_R are plotted for a given value of η. Also shown is the correlation between R and p_R. This figure means that if we can use the near-infrared spectra to place another constraint on p or η, we will be able to very tightly constrain the range of acceptable values.

3.2. Relative Spectral Behavior

As described by Rivkin, Binzel, & Bus (2005) and Abell (2003), JHK-band spectroscopy of a sufficiently-hot object in the inner Solar System will show the Wien-law tail of the object's thermal emission. The curvature of the spectrum in the transition between the reflected component and the thermal component depends on the object's geometric albedo p and the

beaming parameter η. (Since both components depend on R^2, radius does not matter.) The more (less) reflective the object, the longer (shorter) the wavelength at which the transition occurs. Similarly, the higher (lower) the value of the infrared beaming parameter, the cooler (hotter) the subsolar point is, and the longer (shorter) the wavelength at which the transition occurs. Note in particular that the nucleus's Wien-side of its spectral energy distribution (SED) is very sensitive to the emission from the subsolar point since that is the hottest location on the object. Also, note that generally the subsolar point is hotter than any dust that may reside in the coma, since dust grains are isothermal and often (in Jupiter-family comets) do not have significant superheat (Lisse 2002). Therefore the comet's Wien-side SED is not as susceptible to coma contamination.

The three spectra presented in Paper I are reproduced in our Fig. 3. Each panel shows one spectrum and modeling results (described below). The spectra have had the solar spectrum divided out. It is clear that the color of the nucleus is not flat, i.e. not solar, so the nucleus's geometric albedo depends on wavelength. In our case, the most robust albedo to be obtained from our modeling here is the H-band albedo, p_H. This is because the three spectra show a kink near 1.3 μm and have a constant sloping trend with wavelength only longward of that. Trying to model the kink would not help us constrain the thermal properties of the nucleus; it is likely a real feature and not due to systematic observational problems, but at this point we do not need to understand its origins in order to continue our analysis. We defer further study of this spectral feature to future work. From Paper I (their Fig. 2) we can derive an estimate of the relative reflectance between R-band and H-band: the albedo at H is about 60% higher than at R. Thus p_H must be divided by 1.6 to yield p_R.

Since the spectra are not flat and reflectivity increases with wavelength, we must incorporate a "reddening" slope into the modeling. To determine the appropriate reddening, for each spectrum we fit a linear slope through the data between wavelengths of 1.3 and 1.9 μm. (This avoids the kink and the thermal emission.) We find that the slope is about 0.30 ± 0.02 per micron in the December 3rd spectrum, 0.28 ± 0.02 in the December 10th spectrum, and 0.39 ± 0.03 in the December 11th spectrum. This assumes a reflectance of unity at 1.2 microns. We incorporated these slopes and their uncertainties into the modeling; i.e., we tried various values of the slopes to be sure that the error budget of our final results included an accounting for the uncertainty in the reddening.

We have a two-parameter model with which to analyze the spectra, and the two parameters are p_H and η. The model is similar to that described in the previous subsection. Equation 1b is used to derive the thermal emission. Equation 1a is used for the reflected sunlight but modified to account for the reddening mentioned above; the solar spectrum is simply reddened by the appropriate amount as a function of wavelength (with no reddening

at 1.6 μm). To account for phase angle, we set $G = 0.15$, as derived above, and we incorporated this as Φ_{vis}. Then an overall solar spectrum is divided out to match the presentation in Fig. 3. We modeled each of the three spectra individually, using only wavelengths between 2.0 and 2.4 μm. (Shortward of that, there is no extra information for us; longward of that, the data could be unreliable.) The uncertainty in the reflectance of the December 3rd spectrum was about 0.5% in each spectral bin; of the December 10th spectrum, about 1% in each spectral bin; and of the December 11th spectrum, about 1.5% in each spectral bin. We used these errors in calculating the fit statistic χ^2_ν.

Some example results are shown in Fig. 3, where we have chosen the best fitting value of p_H for three values of η: 0.8, 1.0, and 1.2. As is apparent in the figure, each of these example models adequately fits its respective spectrum. Note that there is good agreement between the model results of the December 3rd and 10th spectra. The results for the December 11th spectrum are somewhat disparate. This could be physically related to the higher reddening slope, but it is likely that the softer curve of the spectrum into the thermal tail is an important effect as well. In any case, as we discuss below, there is no *a priori* reason to disregard the December 11th results, and the differences do not adversely effect our final results too much.

3.3. Synthesis

The two analysis methods give ranges of p and η that intersect in parameter space. By combining the best fits from both methods we can narrow down the allowable range of p_H, p_R, and η. This is shown in the top panel of Fig. 4, where we plot the 1σ contours of p_H and η phase space derived from the near-IR spectral analysis. Each spectrum has its own contour. Note how there is overlap between the results for the three spectra (although there is no single location itself overlapped by all three). Overplotted is the 1σ contour from Fig. 2, but with the albedo scaled up by 60% to account for the difference in R- and H-band albedos. The true albedo and beaming parameter should fall within the overlap of the mid-IR and near-IR results.

This overlap is shown in the bottom panel of Fig. 4. The overlap between the mid-IR contour and each individual near-IR spectrum is shown with a shaded region. The combination of all three shaded regions gives us our answer for the beaming parameter and albedo. We find that $\eta = 1.01 \pm 0.20$ and $p_H = 0.059 \pm 0.023$. This corresponds to $p_R = 0.037 \pm 0.014$. For reference, from Fig. 2 in Paper I we find that p_R is 9% higher than p_V, therefore $p_V = 0.034 \pm 0.013$. Using our Fig. 2, and the allowed range of η, the effective radius of 162P's nucleus is $R = 6.0 \pm 0.8$ km.

4. Discussion

4.1. Absolute Magnitude and Phase Slope Parameter

As mentioned, we have derived a value for the R-band absolute magnitude H_R based on photometry that covers a range of phase angles. However the rotational context is not known, and for a proper analysis of the phase law, one needs to account for the variability of the magnitude due to the nucleus's rotation. Our lack of this information introduces an uncertainty into our derivation of H_R and G. There is a possibility that if the nucleus's light curve amplitude is large then we are being fooled, and these two quantities may have quite different values.

In particular this is a concern because a slope parameter of $G = 0.15$ is somewhat higher than has been found for several other cometary nuclei and outer Solar System objects (Fernández et al. 2000; Schaefer & Rabinowitz 2002; Sheppard & Jewitt 2002; Bauer et al. 2003; Jewitt & Sheppard 2004), although it is comparable to that found by Buratti et al. (2004) for comet 19P/Borrelly. The problem is compounded by the fact that the mid-IR and near-IR observations both took place at moderate phase angle (46° and 49°). If 162P's slope parameter is indeed much smaller than 0.15, this would mean that H_R is brighter than we have calculated. This, in turn, would mean that the nucleus's true albedo is higher and effective radius is lower than we have derived here. For example, if the nucleus's $G = -0.05$, then the infrared observations would imply that $p_R \approx 0.06$ and $p_H \approx 0.09$. Such an albedo would be somewhat higher than the other albedos known for Jupiter-family comets (Lamy et al. 2005), and be closer to those of Centaurs and transneptunian objects (Stansberry et al. 2005). Furthermore the effective radius would be $R \approx 4.7$ km, admittedly still a fairly large nucleus.

4.2. December 11th Spectrum

The fact that the December 11th spectrum is somewhat different from those of the other dates suggests that we should explore why this may be. First we can check the rotational context of the observations. The rotation period of the comet is about 32.78 hours (G. Masi, private communication), so we can calculate the relative rotational phase between the four epochs. If the December 3rd spectrum occurred at rotational phase $\phi = 0$, then at the other epochs, $\phi = 0.13$ for the December 10th spectrum, $\phi = 0.32$ for the December 11th spectrum, and $\phi = 0.59$ for the December 27th photometry. Therefore there is no clear conclusion we can draw about what effect the rotation may have had on our interpretation of the modeling results. For example if the December 11th spectrum had been at a much different rotational

phase compared to the other three datasets, then we would have reason to disregard it in the final analysis, but this is not the case. (We admit that if the rotation period is wildly off from 32.78 hours then we will have to readdress this argument.) In any case the lack of rotational context for the visible-wavelength photometry introduces extra uncertainty in the problem.

Another explanation may be secular changes in the comet's activity. For example, perhaps there was an outburst of activity sometime between December 10.25 and December 11.88. This would have formed a dust coma that would affect the spectral measurements. If the dust grains had sizes that were approximately 1 to 10 μm in scale, then they would have contributed extra reflected sunlight but little thermal emission in K-band. This is because the grains would have been isothermal and would not have reached the hotter temperatures that are achieved at and near the nucleus's subsolar point. Modeling such a spectrum on the assumption that we were only seeing light from the nucleus would yield higher albedos than normal – which is exactly what is seen in the December 11th spectrum. If this scenario is correct, then we should not include this spectrum in the derivation of the properties of the nucleus.

Finally, we note that the signal-to-noise ratio (S/N) of the spectrum on December 11th is somewhat lower than that from December 3rd and 10th. The S/N of this spectrum is still good and cannot be rejected for that reason, but if we were to take just the two higher S/N spectra we would find that the acceptable range of η is 0.98 ± 0.17 (as can be found from Fig. 4). This is not too different from our solution in §3.3. Furthermore there would be no difference in our range of acceptable albedos p_H (as can also be seen from Fig. 4). The acceptable range of radii R would shrink by only a few tenths of a kilometer (as can be seen from Fig. 2).

In short, there is no conclusive evidence letting us explain why the December 11th spectrum is different, and also no strong reason why it should be removed from consideration.

4.3. Thermal Properties

Only recently have there been sufficient thermal measurements of cometary nuclei that can constrain the thermal inertia. In particular, the thermal emission from the nucleus of 9P/Tempel 1 strongly indicates that the beaming parameter η is near unity, and that the thermal inertia is consistent with zero. This comes from both remote observations by Lisse et al. (2005) and from spacecraft observations reported by A'Hearn et al. (2005) from the *Deep Impact* mission. Soderblom et al. (2004) analyze spatially-resolved *Deep Space 1* near-IR

spectra of comet 19P/Borrelly's nucleus and find that the nucleus's temperature is consistent with a similar thermal behavior. Lastly, observations of comet 2P/Encke by Fernández et al. (2004; and in preparation) indicate that that nucleus has a near unity beaming parameter as well. This is based on mid-IR, near-IR, and visible observations, just as in our present analysis of 162P.

If cometary nuclei are confirmed to commonly have low thermal inertias and near-unity beaming parameters, this will greatly facilitate the interpretation of ground-based mid-IR radiometry. For faint comets often one can detect the comet at only one mid-IR wavelength. This is insufficient to constrain η and so in such a case one needs to assume a value for it. If we know *a priori* that there is a strong likelihood of $\eta = 1$, then this problem is removed. Furthermore one would not necessarily need to obtain time-consuming photometry at many extra wavelengths. A survey of the thermal emission from cometary nuclei would be logistically easier and would yield significant physical information with relatively few model-dependent problems.

We note that our solution for η is fairly low given the phase angle of the observations. Delbó et al. (2003) found an approximately linear relationship between the beaming parameters and phase angles of several near-Earth asteroids (NEAs). Their best-fit line would suggest that η at 46° should be near 1.27. However there is much scatter in their trend and our solution here for 162P is not significantly off. In any case, cometary nuclei likely have different thermal properties anyway. The fact that we do not see an elevated η at such phase angles, unlike what has been seen for many NEAs, is suggestive of this.

4.4. Radius and Albedo Context

A large database of physical information on cometary nuclei was compiled by Lamy et al. (2005). By comparing with this work, our radius for 162P makes it one of the largest Jupiter-family comets (JFCs). Only 28P/Neujmin 1 has an accepted radius that is larger, and 10P/Tempel 2 and 143P/Kowal-Mrkos have comparable radii. This is significant since it was only discovered in October 2004, despite its large size, so perhaps the sample of known JFCs is not as complete as previously thought. Studies of the JFC size distribution by Fernández et al. (1999), Weissman & Lowry (2003), Meech, Hainaut, & Marsden (2004), and Lamy et al. (2005) suggested that we knew about all the nuclei larger than a few kilometers, or at least those with perihelia within roughly 2 AU of the Sun. 162P's perihelion is at 1.2 AU, and its current orbit-intersection distance with Earth is 0.23 AU, so it is a fairly close yet large comet that avoided discovery. While this is partly due to poor apparitions, it also suggests that the comet's weak level of cometary activity – as shown in late 2004 and early

2005 – kept it below the threshold brightness for discovery. The question of our completeness of the JFC sample perhaps needs to be revisited.

The albedo of the nucleus appears to be typical. While the error bar on the albedo is approximately 40%, it overlaps with a significant fraction of the known albedos among JFCs (Lamy et al. 2005). However, it is important to point out that there are only nine other albedos known for JFCs, and that we do not yet have a statistically robust sample with which to make a mathematical comparison.

5. Summary

Mid-infrared observations in December 2004 have let us sample the thermal emission from the nucleus of comet 162P/Siding Spring. In combination with visible-wavelength photometry reported by Hergenrother (2006) and three near-infrared spectra reported by Campins et al. (2006) (Paper I), we have calculated the nucleus's effective radius R, geometric albedo p, and beaming parameter η.

We used a two-pronged analysis where we constrained all three quantities with the mid-IR and visible data, and then independently constrained p and η with the near-IR spectra. The overlap of the ranges of acceptable (1σ) values for these quantities lets us derive a beaming parameter of $\eta = 1.01 \pm 0.20$, and a geometric albedo of $p_H = 0.059 \pm 0.023$ and $p_R = 0.037 \pm 0.014$ in H- and R-band respectively. We also find that the effective radius at the time of the December 27th observations was 6.0 ± 0.8 km.

There are two significant conclusions. First, we find that the nucleus is one of the largest known among Jupiter-family comets. This suggests that we must be cautious in understanding the completeness level to which we have discovered all JFCs. Second, with a beaming parameter near unity, this continues a trend of finding little infrared beaming among cometary nuclei. If this property is widespread, radiometric observations of cometary nuclei will be much easier to interpret and less prone to model dependencies.

We are indebted to the support team at IRTF for making these observations possible. Our work benefited from the very thorough analysis by an anonymous referee. We acknowledge the JPL SSD group for their very useful "Horizons" ephemeris service. This work was supported in part by a SIRTF Fellowship to YRF. HC acknowledges support from grants from NASA's Planetary Astronomy program and from the National Science Foundation.

REFERENCES

Abell, P. A. 2003, Ph. D. Thesis, Rensselaer Polytechnic Inst., Troy, NY

A'Hearn, M. F., & 32 colleagues, 2005, Science, 310, 258

Allen, D. A. 1970, Nature, 227, 158

Bauer, J. M., Meech, K. J., Fernández, Y. R., Pittichova, J., Hainaut, O. R., Boehnhardt, H., & Delsanti, A. C. 2003, Icarus, 166, 195

Bowell, E. , Hapke, B., Domingue, D., Lumme, K., Peltoniemi, J., & Harris, A. W. 1989, in Asteroids II, ed. R. P. Binzel et al. (Tucson: Univ. of Arizona Press), 524

Buratti, B. J., Hicks, M. D., Soderblom, L. A., Britt, D., Obsert, J., & Hillier, J. K. 2004, Icarus, 167, 16

Campins, H., Ziffer, J., Licandro, J., Pinilla-Alonso, N., Fernández, Y., de León, J., Mothé-Diniz, Th., & Binzel, R. P. 2006, AJ, in press (Paper I)

Cohen, M., Witteborn, F. C., Carbon, D. F., Davies, J. K., Wooden, D. H., & Bregman, J. D. 1996, AJ, 112, 2274

Delbó, M., Harris, A. W., Binzel, R. P., Pravec, P., & Davies, J. K. 2003, Icarus, 166, 116

Deutsch, L., Hora, J., Adams, J., & Kassis, M. 2002, SPIE, 4841, 106

Engelke, C. W. 1992, AJ, 104, 1248

Fernández, J., Tancredi, G., Rickman, H., & Licandro, J. 1999, A&A, 352, 327

Fernández, Y. R., Lisse, C. M. Käufl, H. U., Peschke, S. B., Weaver, H. A., Lamy, P. L., Livengood, T. A., & Kostiuk, T. 2000, Icarus, 147, 145

Fernández, Y. R., Lisse, C. M., Schleicher, D. G., Bus, S. J., Kassis, M., Hora, J. L., & Deutsch, L. K. 2004, BAAS, 36, 2104 [abstract]

Harris, A. W. 1998, Icarus, 131, 291

Harris, A. W., & Davies, J. K. 1999, Icarus, 142, 464

Harris, A. W., Davies, J. K., & Green, S. F. 1998, Icarus, 135, 441

Hergenrother, C. 2006, Icarus, submitted

Jewitt, D., & Sheppard, S. 2004, AJ, 127, 1784

Lamy, P. L., Toth, I., Fernández, Y. R., & Weaver, H. A. 2005, in Comets II, ed. M. Festou, H. U. Keller, & H. A. Weaver (Tucson: Univ of Arizona Press), 223

Lebofsky, L. A., & Spencer, J. S. 1989, in Asteroids II, ed. R. P. Binzel et al. (Tucson: Univ. of Arizona Press), 128

Lebofsky, L. A., Sykes, M. V., Tedesco, E. F., Veeder, G. J., Matson, D. L., Brown, R. H., Gradie, J. C., Feierberg, M. A., & Rudy, R. J. 1986, Icarus, 68, 239

Lisse, C. 2002, EM&P, 90, 497

Lisse, C. M., A'Hearn, M. F., Groussin, O., Fernández, Y. R., Belton, M. J. S., van Cleve, J. E., Charmandaris, V., Meech, K. J., & McGleam, C. 2005, ApJ, 625, L139

Matson, D. K. 1971, Ph. D. thesis, California Institute of Technology

Meech, K. J., Hainaut, O. R., & Marsden, B. G. 2004, Icarus, 170, 463

Morrison, D. 1973, Icarus, 19, 1

Rivkin, A. S., Binzel, R. P., & Bus, S. J. 2005, Icarus, 175, 175

Schaefer, B. E., & Rabinowitz, D. L. 2002, Icarus, 160, 52

Sheppard, S. S., & Jewitt, D. C. 2002, AJ, 124, 1757

Soderblom, L. A., Britt, D. T., Brown, R. H., Buratti, B. J., Kirk, R. L., Owen, T. C., & Yelle, R. V. 2004, Icarus, 167, 100

Stansberry, J. A., Cruikshank, D. P., Grundy, W. G., Margot, J. L., Emery, J. P., Fernández, Y. R., & Rieke, G. H. 2005, BAAS, 37, 5205 [abstract]

Weissman, P. R., & Lowry, S. C. 2003, in Lunar and Planetary Science Conference XXXIV, Abstract #2003, LPI, Houston [CD-ROM]

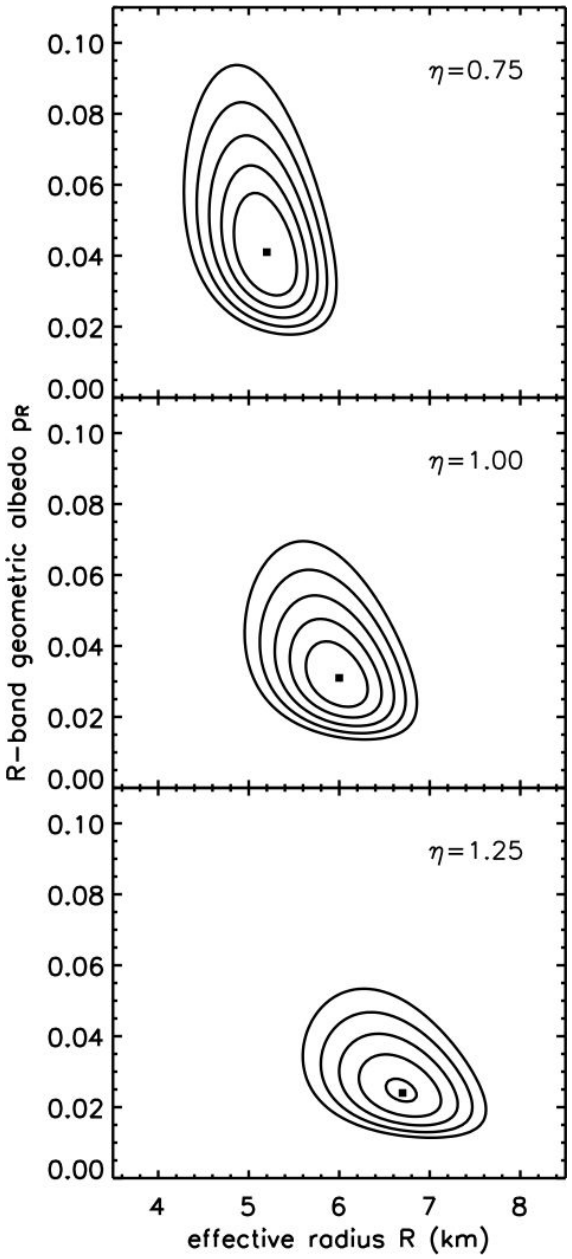

Fig. 1.— Contour plots of the fit statistic χ^2_ν after modeling the mid-IR photometry and visible absolute magnitude. We have represented the three-dimensional nature of χ^2_ν by showing three representative values of the beaming parameter η: 0.75, 1.0, and 1.25. In each plot, the five contours represent the 1, 1.5, 2, 2.5, and 3-σ contours. The filled square shows the lowest χ^2_ν for that particular value of η. A wide of range of R, p_R and η are viable solutions.

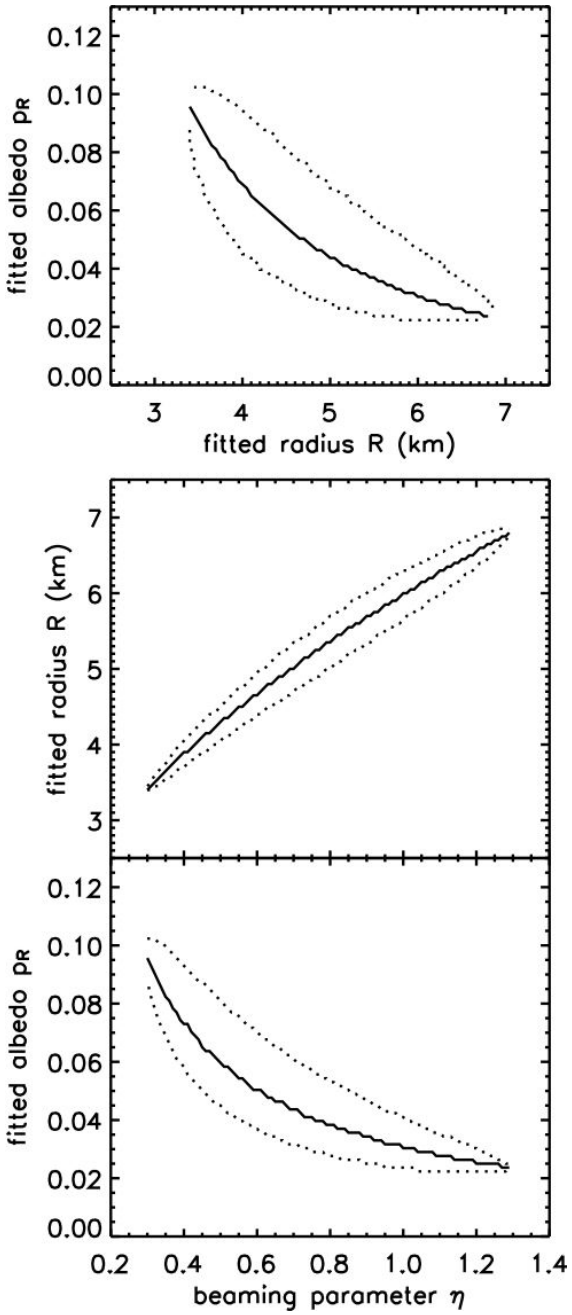

Fig. 2.— Plots showing the correlation between the three parameters that were fit, R, p_R, and η. Dotted lines represent the 1-σ ranges. The jagged nature of the curves is due to the quantization of the sampling of parameter space. While Fig. 1 shows that each parameter individually has a wide range of possible values, the plots here show that the values are strongly correlated. Another constraint on any one of these parameters will yield a dramatic decrease in the error bar associated with all three.

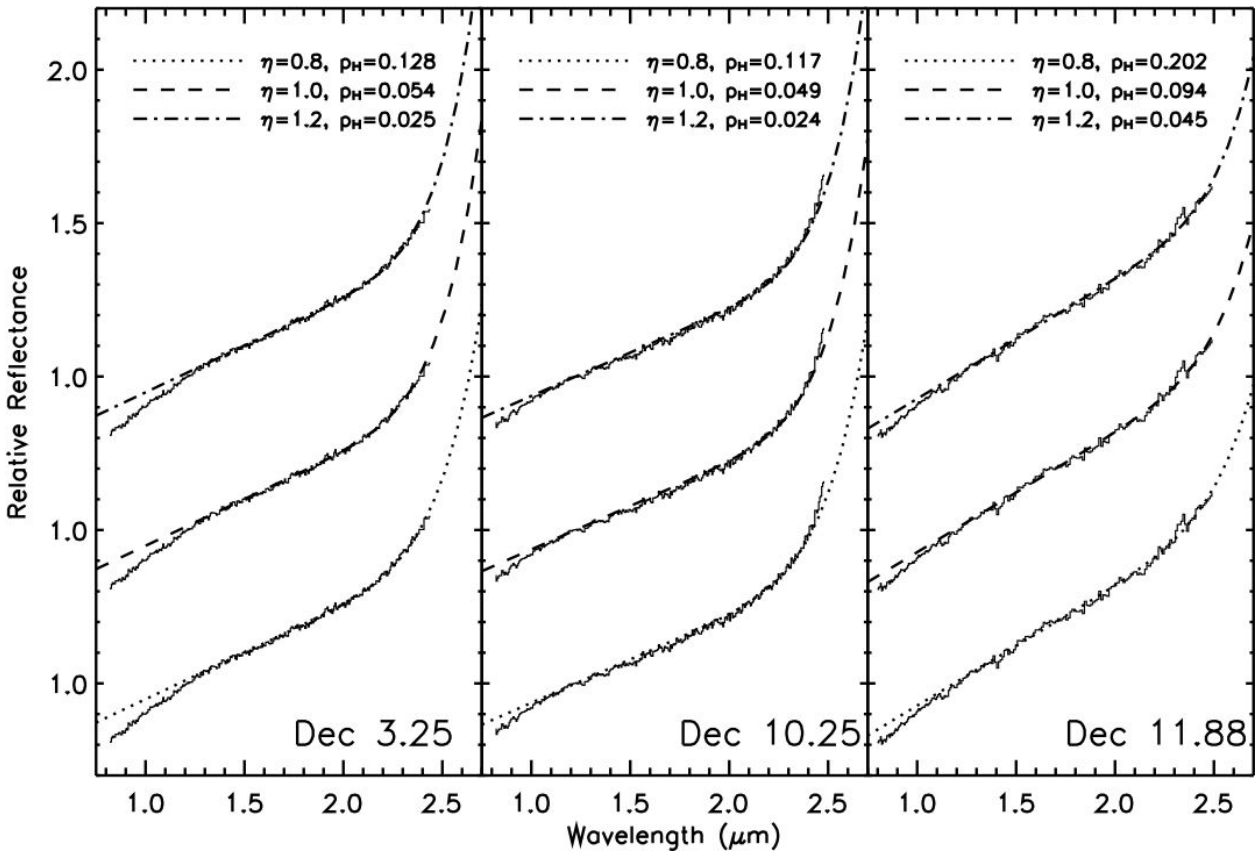

Fig. 3.— Model results of the three spectra presented in Paper I. Each panel represents one spectrum, with the date of that spectrum given at bottom right. Three example models are shown for each spectrum, and the spectrum has been offset from itself for clarity. The model parameters, η and p_H are written at top. To calculate the fit statistic for a model, we used an error bar of 0.5%, 1%, and 1.5% on the reflectance of each spectral bin in the December 3rd, 10th, and 11th spectra, respectively. As with the mid-IR analysis, a wide range of values satisfy the spectra. Note however that generally higher albedos are needed for the December 11th spectrum.

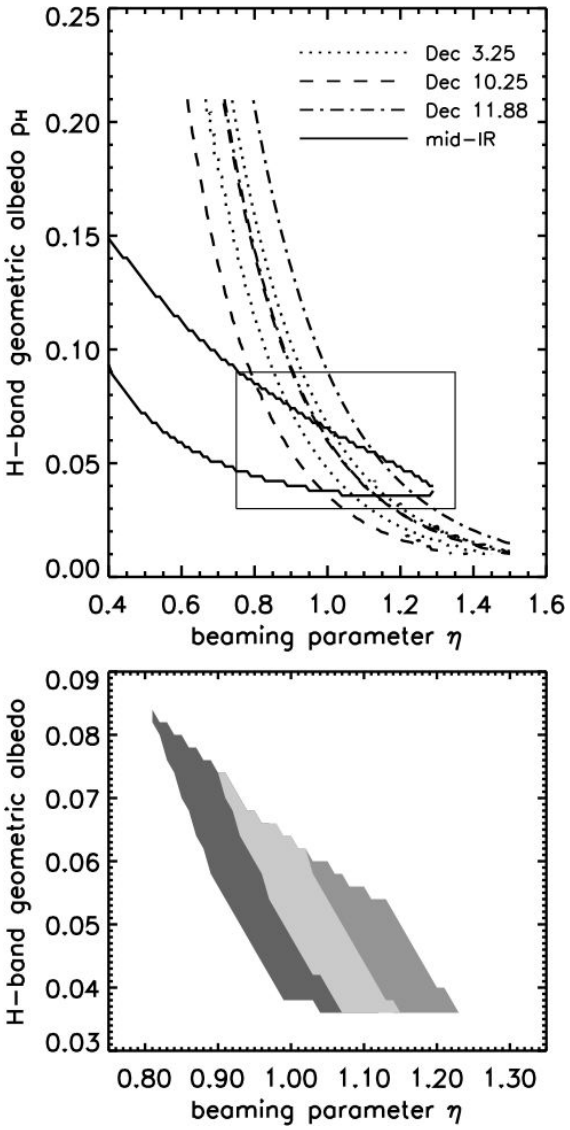

Fig. 4.— Top: Contour plot of the 1σ boundaries for p_H and η as derived from fitting the three near-IR spectra. The model results for each spectrum are shown. The parameter spaces of the three spectra overlap. Overplotted is the 1σ region from Fig. 2 showing the mid-IR constraint on p_H and η. We have scaled up p_R by 60% in order to compare it to the p_H here. The rectangle shows the area encompassed by the bottom panel. Bottom: Shaded regions showing various overlaps, showing how we derive the allowable ranges to p and η. The lightest, darkest, and middle grey indicate overlap between the mid-IR results and the spectrum results from December 3rd, 10th, and 11th, respectively (though the December 3rd region is on top, covering some of the overlaps of the other two dates). Our estimate of the nucleus's η and p_H comes from the extent of this entire shaded region.